Evaluating the influence of mechanical system vibration characteristics on servo motor efficiency

Rigacci, Massimiliano

Sato, Ryuta

Shirase, Keiichi

(Citation)
Precision Engineering,72:680-689

(Issue Date)
2021-11

(Resource Type)
journal article

(Version)
Accepted Manuscript

(URL)
https://hdl.handle.net/20.500.14094/90008718

Evaluating the Influence of Mechanical System Vibration Characteristics on Servo Motor Efficiency

Massimiliano Rigacci, Ryuta Sato, and Keiichi Shirase

Department of Mechanical Engineering, Kobe University, 1-1 Rokkodai, Nada, Kobe, 657-8501, Japan

Abstract

In this study, the influence of mechanical vibration characteristics on the efficiency of a servo motor was experimentally investigated. For this purpose, a dedicated apparatus comprising two servo motors connected to a coupling was used. The efficiency of the motor was investigated by first considering the signals of voltage and current; then, the mechanical power was calculated from the acquired torque and angular velocity supplied by the motor. Subsequently, working conditions involving different angular velocities and loading torques were investigated to generate a motor efficiency map. To clarify the influence of the vibration characteristics on the motor efficiency, two types of couplings differing in torsional stiffness and damping characteristics were considered—Type A and Type B. The efficiency was calculated for eight vibration conditions imposed via the selection of the velocity control gain settings for both types. Resultantly, the manner in which the efficiency is affected by the vibration conditions was clarified. Moreover, coupling in the case of better vibration damping characteristics was confirmed to yield a higher motor efficiency for all gain settings. Furthermore, motor working conditions corresponding to high and low motor efficiencies were evaluated, and the motor thermal behavior was investigated. Overall, a lower motor efficiency was confirmed to be associated with increasing temperatures. These results suggest the importance of the vibration characteristics of mechanical systems for achieving high efficiency.

Keywords; Motor efficiency, Mechanical vibration, Power consumption, Coupling

1. Introduction

The topic of motor efficiency has long attracted significant research attention; however, in recent years, well-known issues related to increasing human resource consumption have emphasized the importance of efficient energy usage. Electric motors are among the most common machines used in industry and daily life; therefore, determining the optimal working conditions to obtain the highest possible efficiency is critical. In this regard, several methods have been proposed to improve the efficiency of electric motors, among which at least two types can be identified: methods based on control strategies, and methods based on design to achieve high efficiency. A discussion on the state-of-the-art methods for loss minimization was presented in [1]; of these methods, those based on mathematical functions of the losses were developed in [2]. Other methods based on adaptive routines—such as maximization of the active power through control variable adjustment—were proposed in [3], and the maximum torque per ampere strategy was proposed by [4]. Elsewhere, analytical and finite element design methods targeting optimum rotor shapes for achieving high-efficiency line start permanent magnet motors were developed in [5], and a design method to maximize the efficiency of an interior permanent magnet synchronous motor (PMSM) was developed in [6]—this method employed a genetic algorithm to find the optimal flux density and direct and quadrant axis inductances. Therefore, significant focus has been placed on motor efficiency improvement; however, while motor efficiency is one of the desirable and important characteristics of electric motors, low-torque oscillations constitute another. In an internal permanent magnet motor, the motor torque can cause vibration owing to the cogging torque, radial force, and commutation torque ripple, which are all electromagnetic sources of vibration. Thus, design methods for minimization of torque vibration based on rotor shape were proposed in [7]. In the last twenty years, the advent of hybrid cars has emphasized the importance of low-vibration torque motors [8]; a method for computing the vibration response under various operating

conditions was developed in [9]. The aforementioned studies involved the development of methods to predict and minimize torque vibrations due to electromagnetic sources; thus, the attention in these studies was placed only on the electric motor as a source of torque vibration. However, in many common applications, torque vibrations can also be derived from the mechanical system to which the motor is joint. The vibrating load torque can be induced by an unbalanced rotor of the system driven by an electric motor [10]. In this regard, some researchers have proposed an active control force method for the attenuation of vibration mass imbalance in rotor-bearing systems [11, 12].

In the machine tool field, an investigation of how vibrating load torques affect feed drive systems was conducted in [13], while the effect of chatter vibration on spindle motor torque was elucidated in [14]. However, in both these cases, suppression of torque vibration by means of varying the working conditions was the main focus, and the effect of vibrations on the motor efficiency was not considered. On the other hand, studies on motor efficiency, where no significant torque vibrations occur, were conducted in [15-17]. For common applications such as feed drive systems, the motor efficiency and total feed drive system power consumption have been experimentally investigated [18, 19].

In most industrial applications, such as feed drive systems, electric motors are connected to other components through couplings (or joints); therefore, the dynamic characteristics of the coupling are also considered important. Coupling characteristics and control system gain have been shown to strongly affect the vibrational behavior of the system [20]; therefore, they affect the characteristics of the torque supplied by the motor. Manufacturers of such motors always attempt to achieve higher control gains for the feedback controllers to yield a higher response of the system, although there exists the possibility of wasting energy owing to unexpected vibrations. However, to the best of the authors' knowledge, the effects of vibrational characteristics on the output of servomotors have not been sufficiently examined. Further investigations are required on the effect of motor coupling characteristics on motor efficiency, especially for increasing oscillation magnitudes of the torque and velocity.

This study therefore presents an experimental investigation of motor efficiency, aiming to clarify whether torque vibrations affect motor efficiency; therefore, this research focuses on the relationship between efficiency and oscillation magnitude. Elucidating the effect of vibrations on motor efficiency can encourage designers to design more sophisticated control techniques for suppression of vibration and reduction of motor power consumption. Moreover, investigating the relationship between motor efficiency and torque vibrations represents the first step towards the development of methods for machine condition assessment through efficiency monitoring, which has significant potential, particularly with respect to the Internet of Things revolution.

Therefore, to this end, a dedicated apparatus comprising two PMSMs was analyzed, and the motor efficiency thereof was investigated under several load and velocity conditions. Two coupling types—Type A and Type B—were tested using the apparatus, with each type exhibiting distinct dynamic characteristics. Then, the motor efficiency was measured according to the working conditions determined by each coupling. To clarify the effect of torque oscillations on motor efficiency, the torque oscillation magnitude was controlled by adjusting the value of the proportional constant of the velocity loop. Type B was found to maintain a high motor efficiency through oscillation suppression, whereas Type A was observed to exhibit relatively poor performance. The motor thermal behavior was investigated using a thermocouple, and it was confirmed that at a fixed mechanical power output, the temperature of the low-efficiency motor increased more than that of the high-efficiency motor. Overall, this study emphasizes the importance of high damping component selection to suppress vibrations and achieve high efficiency while maintaining a high control gain.

2. Experimental apparatus and measurement methods

2.1. Description of apparatus

The apparatus used in this study is shown in Figure 1. It consists of two servo motors, Servo Motor A (left) and Servo Motor B (right). Both motors are three-phase PMSMs (Yaskawa SGMGV-05ADA21) with the rated values listed in Table 1. The system was controlled via a personal computer (PC) with a digital signal processor (DSP) board (dSPACE DS1104). Both servo motors were used in the torque control mode, and the servo drivers controlled the torque based on the input voltage signal from the controller. Motor A was controlled using the velocity control loop shown in Figure 2(a), implemented on the DSP board, and the angular velocity was

calculated from the angular displacement detected by the rotary encoder placed on the rear side of the motors. The torque command T_{ref} and angular velocity calculated from the rotational angle were recorded as the torque and rotational speed of the motor, respectively. It was confirmed that the motor torque was precisely controlled by a servo driver with enough high control bandwidth. Servo Motor B was controlled without any feedback control loop, and the torque command signal was directly commanded to the servo driver from the DSP board. The commanded torque to Motor B was in the direction opposite to the rotational direction of Motor A to apply a loading torque to Motor A.

The two motors were positioned to face each other and were connected by a coupling. Two types of couplings were considered in this study—Type A and Type B. Type A coupling was a leaf spring-type coupling characterized by high torsional stiffness, and Type B was a laminated rubber coupling characterized by high damping characteristics. The schematics of both couplings are presented in Figure 3.

2.2. Measurement of electric quantities

The electric power consumption of the motor was determined in terms of the voltage and current, which were calculated according to the method depicted in Fig. 4. The voltage across the two phases was measured using differential probes, while the current along each phase was measured using amperometric clamps. The motor was a three-phase motor; however, because no neutral wire was used, it was sufficient to measure two differential voltages and two currents, as expressed in Eq. (1):

$$\begin{gathered} P = E_1 I_1 + E_2 I_2 + E_3 I_3 = W_a + W_b + W_c \\ I_1 + I_2 + I_3 = 0 \\ P = E_1 I_1 + E_2(-I_1 - I_3) + E_3 I_3 \\ P = (E_1 - E_2) I_1 + (E_3 - E_2) I_3 = V_{12} I_1 + V_{32} I_3 = W_a + W_b, \end{gathered} \tag{1}$$

where E_1, E_2, and E_3 are the voltages of each phase; I_1, I_2, and I_3 are the currents of each phase; and W_a, W_b, and W_c are the electric powers of each phase. Moreover, the voltage and current signals were amplified and filtered using a low-pass filter with a cutoff frequency of 1600 Hz. Data acquisition and motor control were performed using a PC with a DSP board (dSPACE DS1104) at a frequency of 4000 Hz for 0.5 s, implying that the number of acquired points, n, was 2000. Once the signals were acquired, the apparent electric power was calculated using Eq. (2):

$$\begin{gathered} V_{rms} = \sqrt{\frac{1}{n}\sum_{k=1}^{n}\{V_k\}^2} \\ I_{rms} = \sqrt{\frac{1}{n}\sum_{k=1}^{n}\{I_k\}^2} \\ P_{app}^{e} = \sum_{k=1}^{2} V_{rms}^{k} * I_{rms}^{k}, \end{gathered} \tag{2}$$

where n is the number of acquired points; V_k and I_k are the *k-th* voltage across the two phases and the current along the phase, respectively; V_{rms} and I_{rms} are the respective relative root mean squares of the aforementioned parameters; and P_{app}^{e} is the apparent electric power. The apparent power was considered as the reference for electric power consumption owing to the contribution of the reactive power to the motor heat generation [21, 22].

2.3. Measurement of mechanical quantities

The mechanical quantities considered in this analysis were calculated using Eq. (3). The angular velocity was acquired via the rotary encoder, while the torque was acquired directly from the control system.

$$\begin{aligned}
\tau_{ave} &= \frac{1}{n}\sum_{k=1}^{n}\tau_k \\
\omega_{ave} &= \frac{1}{n}\sum_{k=1}^{n}\omega_k \\
\tau_{oscill} &= \frac{1}{n}\sum_{k=1}^{n}(\tau_k - \tau_{ave}) \\
\omega_{oscill} &= \frac{1}{n}\sum_{k=1}^{n}(\omega_k - \omega_{ave}) \\
P^m_{main} &= \tau_{ave} * \omega_{ave} \\
P^m_{oscill} &= \frac{1}{T}\int \tau_{oscill}(t) * \omega_{oscill}(t)dt \\
P^m_{overall} &= \frac{1}{T}\int \tau(t) * \omega(t)dt,
\end{aligned} \tag{3}$$

where τ_k and ω_k are the torque and angular velocity, respectively; P^m_{main} is the main mechanical power supplied by the motor; P^m_{oscill} is the power associated with the oscillating component of the signals; and $P^m_{overall}$ is the overall mechanical power, which is the sum of P^m_{main} and P^m_{oscill}.

2.4. Efficiency calculation method

The efficiency of the motor was calculated using Eq. (4).

$$\eta_e = \frac{P^m_{main}}{P^e_{app}} = \frac{\tau_{ave}\omega_{ave}}{\sum_{k=1}^{2} V^k_{rms} * I^k_{rms}}. \tag{4}$$

The main component of the power was considered as the useful output of the motor, while the apparent electric power was considered as the input. Thus, oscillations of the output power due to dynamic phenomena were not considered as useful outputs.

3. Motor efficiency evaluation

3.1. Measurement method

To evaluate the motor efficiency, a total of 360 test conditions were investigated. Each test was conducted as per the following procedure: A constant load torque was applied through motor B, while a set of angular velocities was commanded through motor A. The set of velocities comprised 24 angular velocities between 1 and 65 rad/s (approximately 9 and 620 rpm). A total of 15 load torques between 0.05 Nm and 2.7 Nm were applied to each set

of velocities. Because Motor B was set in the torque control mode, each load torque was imposed by inputting the desired torque value directly from the DSP board. For each velocity value, clockwise and counterclockwise directions of rotation were considered; positive and negative load torques were considered as well. For each test, the signals were acquired for 0.5 s during the constant-velocity motion, and only the case in which the load torque opposed the relative velocity was considered. Finally, the efficiency was calculated using Eq. (4) as the average of the clockwise and counterclockwise rotation efficiencies. An example of signals of angular velocity, torque, voltage, and current is shown in Fig. 5 and Fig. 6 for a rotation of 39 rad/s and load torque of 1.2 Nm, and a more detailed description of the test condition is reported in [18]. Through these tests, an efficiency map of the system motor coupling was generated. The measurements were performed considering four values of the proportional gain of the velocity control loop (K_{vp}): 0.10, 0.15, 0.30, and 0.60. Thus, four efficiency maps were generated for each coupling. Because two coupling types were considered in this study, eight efficiency maps were generated to account for eight distinct sets of dynamic conditions.

The two coupling types differed in terms of torsional stiffness and damping characteristics. Notably, the damping characteristics of the joint motor coupling were strongly affected by the tightening torque and contact condition between the coupling and motor shaft. Therefore, to obtain consistent measurements in terms of torque oscillation magnitude, the tightening torque had to be controlled, and the apparatus had to be used for 3 h before the test to measure efficiency was commenced. Further details pertaining to the relationship between damping and tightening torque are available in [23].

3.2. Evaluated efficiency

Figure 7 shows the efficiency map for K_{vp} = 0.15 in the case of Type A coupling. According to the results, the efficiency of the motor strongly depends on the rotating velocity and loading torque of the motor. A high motor efficiency was achieved at high rotating velocities and moderate torques, while the efficiency decreased significantly when the angular velocity was low.

4. Influence of vibration characteristics on torque and efficiency

4.1. Torque oscillations

Figure 8 shows the torque signal for a velocity of 39 rad/s and a load torque of 1.2 Nm for Type A. Figure 8(a) shows that the oscillation magnitude was very small for the lowest K_{vp} considered. The torque oscillation magnitude increased with K_{vp} until the system became unstable, as shown in Figure 8(c); further, torque became fully saturated in the case shown in Figure 8(d). Figure 9 shows the torque oscillation magnitude for Type B; the torque oscillations were very limited for all four K_{vp} values considered, owing to the high damping characteristics of the coupling.

4.2. Motor efficiency variation according to oscillation conditions

The effects of the torque oscillations on the efficiency of the motor with Type A and Type B couplings are shown in Figures 10 to 13. The efficiency maps in Figure 10 show that, for K_{vp} = 0.10, the motor functioned efficiently for a wide range of torques and angular velocities under both coupling cases considered. Figures 11–13 show that the efficiency decreased in the case of Type A coupling, especially for low angular velocities, because the torque oscillation magnitude increased, as shown in Figure 8. Figures 12 and 13 clearly show the efficiency differences between the two cases. Increasing the K_{vp} values for the Type A coupling significantly decreased the efficiency, whereas the efficiency was not notably affected in the case of the Type B coupling. This phenomenon occurred because the high damping characteristic of the Type B coupling greatly limited the onset of torque and velocity oscillations; therefore, the motor energy consumption and efficiency were not affected by the raised K_{vp}. This finding shows that the system efficiency is affected by the oscillation level of the motor torque and does not actually depend on the gain settings.

In addition, it is expected that the input energy from the motor was dissipated, especially from the Type B coupling, and affected the efficiency map. From this standpoint, the power dissipation due to damping can be expressed as a function of the oscillation magnitude according to $W_s = -\alpha X_0^2$ in the case of structural damping, and $W_v = -c\pi\omega X_0^2$ in the case of viscous damping; X_0^2 is the square oscillation magnitude, α and c are constants, and ω is the vibration pulsation. For the Type B coupling, the damping characteristics were so prominent that they reduced the oscillation magnitude to a very small value; therefore, even though the damping coefficient was higher, the non-oscillating condition led to very small power dissipation. However, a comparison of the energy dissipation among different types of couplings needs to be conducted to gain a deeper understanding of the energy flow involved. This will be attempted in future work.

5. Power analysis

5.1 Oscillation power

To understand the motor efficiency behavior under oscillation, the velocity and torque signals were decomposed into main and oscillating components. Figure 14(a) shows the motor A angular velocity when a constant angular velocity of 33.5 rad/s was commanded and K_{vp} = 0.30. Figure 14(b) and 14(c) show the angular velocity and oscillating components, respectively. The main component coincided with the averaged angular velocity; the oscillating component had a zero average, and its magnitude strongly depended on K_{vp}. The oscillating component represents the deviation of the motor angular velocity from the commanded value; therefore, because the motor A angular velocity was controlled, the control applied a restoring torque to neutralize the deviation. Figure 15 shows the angular velocity and torque signals for the four K_{vp} values considered. Torque oscillation affected the velocity oscillation, and the oscillation magnitude increased with K_{vp}. As shown in Figure 15(a), the oscillation magnitude is considered null; because the oscillating power did not represent a useful output, the motor provided minimum power. Therefore, the motor achieved the highest efficiency (Fig. 10). Figure 15(b) to (d) show that the torque and angular velocity were out of phase by 180°. This phenomenon occurred because the velocity control involved application of torque to neutralize the deviation when the angular velocity deviated from the commanded value. Thus, whenever a deviation occurred, a restoring torque was applied. In terms of power, this means that the motor had to perform additional work to neutralize the oscillation and maintain the velocity at the commanded signal. The power required to neutralize the oscillations was calculated using Figure 15 and Eq. (3) Because the oscillating components of angular velocity and torque always have opposite signs, the power associated with the signals was negative; however, from the point of view of the motor, this power is supplied to the system; thus, its sign is positive. Moreover, as K_{vp} increased, the oscillation magnitude increased.

5.2 Power flux analysis

Figure 16 shows the decomposition of the overall mechanical power supplied by the motor into the power associated with the main component and that associated with the oscillating component. The main component represents the power required to handle the load applied by Motor B and the friction; the oscillating component represents the power supplied by the motor to limit velocity oscillations, with no other critical function. As in Figure 16(a), the power associated with oscillation is considered to be null, and the total mechanical power is equal to the main component power. From Figure 16(b) to (d), the oscillating component increased while the main component remained constant, except in Figure 16(d), where the latter was slightly higher. Figure 16 shows the apparent electric power consumed by the motor. The apparent power increased as the velocity and K_{vp} increased. From a mechanical perspective, the apparent power must be increased to provide the motor with sufficient power to suppress oscillations associated with the velocity. From an electrical perspective, it is possible to observe the effect of the velocity oscillations on the voltage and current. Figure 17(a) shows the voltage in the case of low vibration; the voltage oscillated at a specific frequency related to the angular velocity of the motor. As in Figure 17(b), two phenomena were observed: a considerable increase in the voltage magnitude and the presence of two frequencies: The main one related to the angular velocity of the motor, and a higher one directly associated with the frequency of the mechanical vibrations. The shape of the resultant voltage signal was highly distorted, as shown. The considerable growth in the magnitude of the voltage consequently increased the apparent electric power. Thus, the current was also affected by voltage oscillations and apparent power.

5.3 Influence of motor efficiency on increasing temperature

Two thermal tests were performed to confirm the efficiency of the results. The tests involved imposing a constant velocity on Motor A and applying a constant torque through Motor B; specifically, the imposed velocity was 250 rpm, while the torque was 1 Nm. The test conditions were maintained for one hour. A thermocouple was placed on the surface of Motor A, and the motor temperature was measured every 2 s. Two tests were performed: for the first, K_{vp} was set to 0.15, and for the second, it was set to 0.60. The test was initiated after the system temperature was measured for 600 s. Figure 18 shows the results of the tests. Figure 18(a) shows the temperature increase from approximately 27 °C to approximately 32 °C. Figure 18(b) shows the temperature increase from approximately 28 °C to approximately 51 °C. Considering the maps for the cases shown in Figure 10(a) and 13(a) with the aforementioned angular velocity and torque values, it is possible to determine the efficiency under specific working conditions. For the case illustrated in Figure 10(a), the efficiency was approximately 60%, whereas for that in Figure 13(a), it was approximately 21%. Because the mechanical power output was the same in both cases, a difference in efficiency indicates a difference in electric power input, according to Eq. (5):

$$P_{main}^{m} = P_{app}^{e} * \eta_e. \tag{5}$$

The temperature increase depends on the power wastage in the motor, and the ratio of the wasted power is proportional to the ratio of motor efficiency during the test under the same test conditions. Thus, on considering the temperature rise at the beginning of the transient phase (immediately after 600 s) and ignoring heat conduction, convection, and radiation, the steepness of the tangent to the temperature curve represents the speed of the motor heating process. On defining the straight ratio as the ratio of tangents in the two cases, we obtain

$$straight\ ratio = \frac{0.02108}{0.00675} = 3.12. \tag{6}$$

Thus, when K_{vp} = 0.60, the temperature increases more than three times as fast as when K_{vp} = 0.15. The ratio of efficiencies identified from the efficiency maps is

$$efficiency\ ratio = \frac{0.60}{0.21} = 2.86. \tag{7}$$

The straight and efficiency ratios are fairly similar; thus, it was confirmed that the proportionality between the efficiency values was correctly predicted based on the two efficiency maps. Moreover, it was confirmed qualitatively and quantitatively that the low-efficiency motor exhibited higher temperatures than those of the high-efficiency motor for a constant mechanical power output. Finally, as stated in [21] and verified in this study, such a small temperature increase did not affect motor efficiency, indicating that the efficiency at the beginning and end of the experiment remained constant and was determined only by the working condition and K_{vp}.

6. Conclusions

In this study, the efficiency of a PMSM servo motor was experimentally investigated using a dedicated apparatus under several velocity and dynamic conditions. Two couplings with different dynamic characteristics were considered. The following conclusions are drawn.

1) The efficiency of a servo motor strongly depends on the working conditions, such as the angular velocity, torque, and velocity oscillation magnitude.

2) The motor efficiency decreases when the velocity oscillation magnitude increases, especially at low velocities. The dynamic characteristics of the coupling, such as the damping characteristics, strongly influence the oscillation suppression, thus affecting the motor efficiency.

3) The power spent by the motor to limit velocity oscillations, voltage increment, and distortion owing to oscillations are the main causes of reductions in efficiency.

4) The low-efficiency motor exhibits a higher temperature rise than that of the high-efficiency motor, as confirmed through thermal tests.

Overall, this study shows that in practical applications, the efficiency of electric motors is severely affected by the damping characteristics of system components, such as the coupling. Therefore, it serves as guidance for high-efficiency system design through the selection of high damping joints while setting high control gains. Moreover, this study clarifies that there is a close relationship between motor efficiency and vibration level; therefore, it can potentially serve as the first step toward the development of machine condition monitoring methods, such as detection of unpredicted vibration onset through motor efficiency monitoring.

Finally, this study shows that torque vibrations affect the motor heat generation; in machining, 75% of the workpiece geometric errors are related to heat generation [24], which helps to clarify why motor heat generation occurs and how it can be mitigated. In the future, this research will be extended to an investigation of the heat generated by each component, such as coupling, owing to velocity oscillations. Moreover, motor efficiency will be simulated under strong velocity oscillations, and the energy dissipation from the components will be investigated for a deeper understanding of the energy flow involved.

Reference:

1. Cavallaro, C., Oscar, D., Tommaso, A., Miceli, R., Raciti, A., Galluzzo, G.R., Trapanese, M., Efficiency enhancement of permanent-magnet synchronous motor drives by online loss minimization approaches, IEEE Transactions on Industrial Electronics, 52, 4 (2005) 1153-1160.
2. Morimoto, S., Tong, Y., Takeda, Y., Hirasa, T., Loss minimization control of permanent magnet synchronous motor drives, IEEE Transactions on Industrial Electronics, 41, 5 (1994) 511-517.
3. Vaez S., John V. I., Rahman M. A., Adaptive loss minimization control of inverter-fed IPM motor drives, PESC97. Record 28th Annual IEEE Power Electronics Specialists Conference, June (1997), St Louis, MO USA.
4. Lei, Y., Zhang, Y., Huang, W., Accurate and efficient torque control of an interior permanent magnet synchronous motor in electric vehicles based on hall-effect sensors, Energies, 10, 3 (2017)
5. Kim, W.-H., Kim, K.-C., Kim, S.-J., Kang, D.-W., Go S.-C., Lee H.-W., A study on the optimal rotor design of LSPM considering the starting torque and efficiency, IEEE Transactions on Magnetics, 45, 3 (2009) 1808-1811.
6. Sim, D.-J., Cho, D.-H., Chun, J.-S., Jung, H.-K., Efficiency optimization of interior permanent magnet synchronous motor using genetic algorithms, IEEE Transactions on Magnetics, 33, 2 (1997) 1880-1883.
7. Kang, G-H., Hur, J., Kim, W-B., Lee, B_K., The shape design of interior type permanent magnet BLDC motor for minimization of mechanical vibration, IEEE Energy Conversion Congress and Exposition, Sept.(2009) San Jose, CA, USA.
8. Qin, Y., Tang, X., Jia, T., Duan, Z., Zhang, J.,Li, Y., Zheng, L., Noise and vibration suppression in hybrid electric vehicles: State of the art and challenges, Renewable and Sustainable Energy Reviews, 124 (2020) 109782.
9. Saito, A., Suzuki, H., Kuroishi, M., Nakai, H., Efficient forced vibration reanalysis method for rotating electric machines, Journal of Sound and Vibration, 334 (2015) 388-403.
10. Vance, J., Zeidan, F., Murphy, B., Machinery Vibration and Rotordynamics, John Wiley & Sons Inc. (2010)
11. Carbajal, F.B., Tapia-Olvera, R., Valderrabano-Gonzales, A., Yanez-Badillo, H., Rosas-Caro, J.C., Mayo-Maldonado, J.C., Closed-loop online harmonic vibration estimation in DC electric motor systems, Applied Mathematical Modelling, 94 (2021) 460-481.
12. Arias-Montiel, M., Beltran-Carbajal, F., Silva-Navarro, G., On-line algebraic identification of eccentricity parameters in active rotor-bearing systems, International Journal of Mechanical Science, 85 (2014) 152-159.
13. Aslan, D., Altintas, Y., On-line chatter detection in milling using drive motor current commands extracted from CNC, International Journal of Machine Tools and Manufacture ,132 (2018) 64-80.
14. Kakinuma, Y., Sudo, Y., Aoyama, T., Detection of chatter vibration in end milling applying disturbance observer, CIRP Annals - Manufacturing Technology, 60 (2011) 109-112.
15. Peralta-Sanchez, E., Smith, A.C., Rodriguez-Rivas, J.J., Steady-state analysis of a canned line-start PM motor, IEEE Transactions on Magnetics, 47, 10 (2011) 4080-4083.
16. Caricchi, F., Crescimbini, F., Fedeli, E., Noia, G., Design and construction of a wheel directly-coupled axial-flux PM motor prototype for EVs, Proceedings of 1994 IEEE Industry Applications Society Annual Meeting, (1994) Denver, CO, USA.
17. Kurihara, K., Rahman, M.A., High efficiency line-start interior permanent magnet synchronous motors, IEEE Transactions on Industry Applications, 40, 3 (2004) 789-796.
18. Rigacci M., Sato R., Shirase K., Experimental evaluation of mechanical and electrical power consumption of feed drive systems driven by a ball-screw, Precision Engineering 64 (2020) 280-287.
19. Hayashi, A., Sato, R., Iwase, R., Hashimoto, M., Shirase, K., Measurement and simulation of electric power consumption of feed drive systems, Proceedings of the ASME 2013 International Mechanical Engineering Congress and Exposition, (2013) San Diego, CA, USA.
20. Nagao A., Sato R., Shirase K., Influence of torsional damping and lead of ball-screw onto vibration characteristics of feed drive system, Proceedings of International Conference on Leading Edge Manufacturing in 21st century: LEM21 2017.
21. Ma, K., Liserre, M., Blaabjerg, F., Reactive power influence on thermal cycling of multi-MW wind power inverter, IEEE Transactions on Industry Applications, 49 2 (2013) 922-930
22. Akagi, H., Watanabe, E. H., Aredes, M., Instantaneous power theory and applications to power conditioning, IEEE Press Wiley, Second Edition (2017).
23. Nanda, B. K., Study on the effect of bolt diameter and washer on damping in layered joint structures, Journal of Sound and Vibration 290 (2006) 1290-1314.
24. Li, Z-J., Zhao, C-y., Lu, Z-c, Thermal error modeling method for ball screw feed system of CNC machine tools in x-axis, The International Journal of Advanced Manufacturing Technology, 106 (2020) 5383-5392.

Figures and Tables:

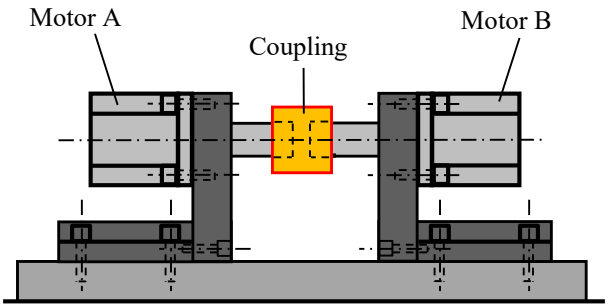

Figure 1 Experimental apparatus

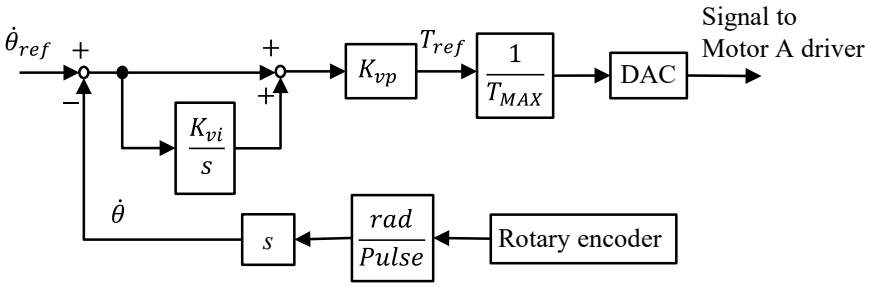

(a) Motor A, velocity control

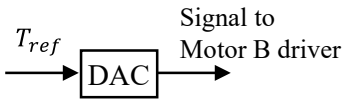

(b) Motor B, torque control

Figure 2 Block diagram of control system for motors

Table 1 Motor specifications

Rated velocity	1500 rpm
Rated torque	2.86 Nm
Rated power	450 W

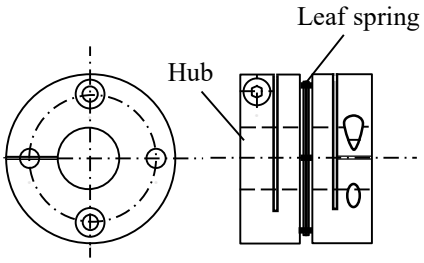

(a) Type A: leaf-spring type.

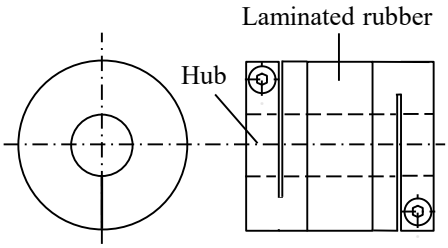

(b) Type B: laminated rubber type

Figure 3 Examined coupling types

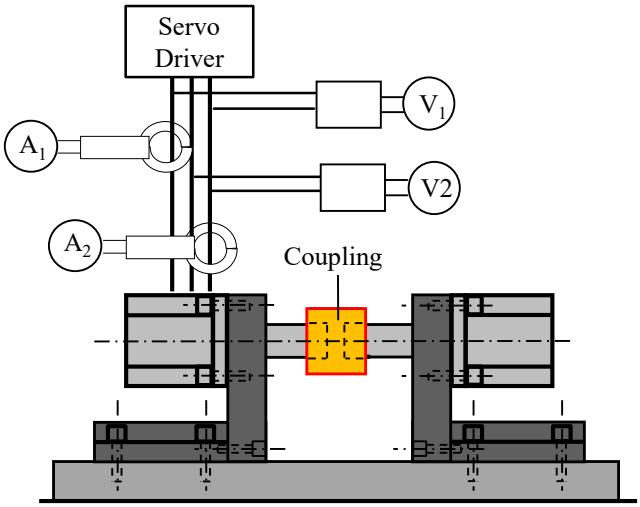

Figure 4 Electric power measurement setup

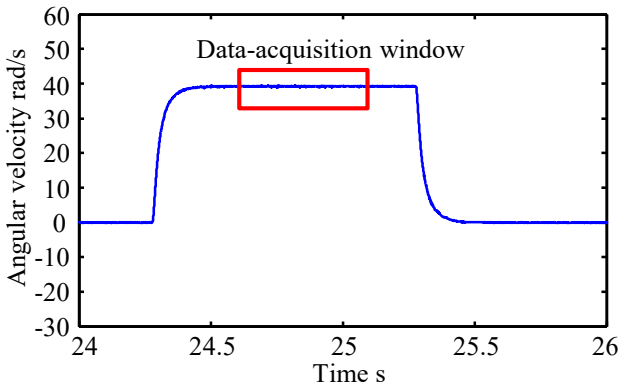

(a) Angular velocity

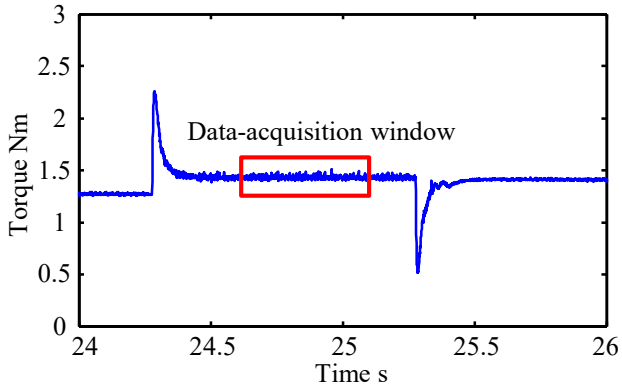

(b) Torque

Figure 5 Example of angular velocity and torque (Type A coupling, K_{vp}= 0.15)

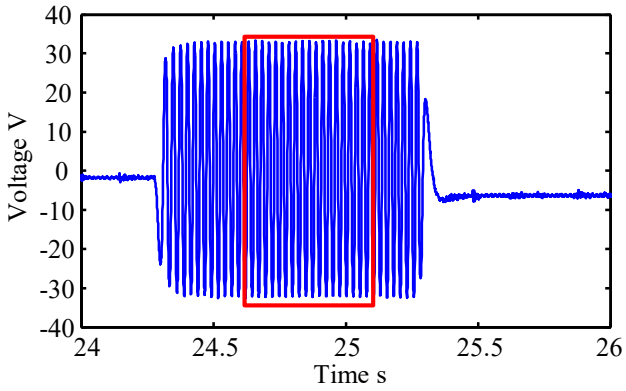

(c) Voltage

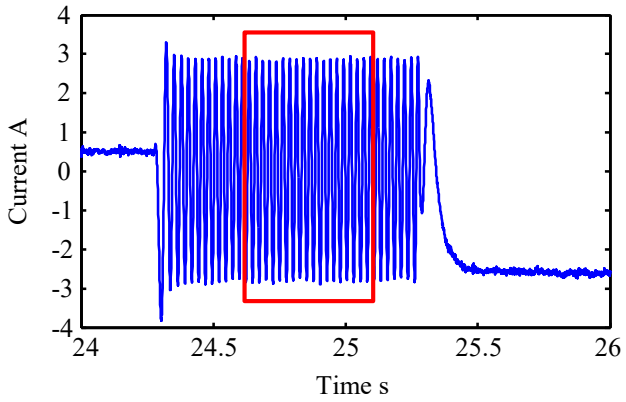

(d) Current

Figure 6 Example of voltage and current (Type A coupling, K_{vp} = 0.15)

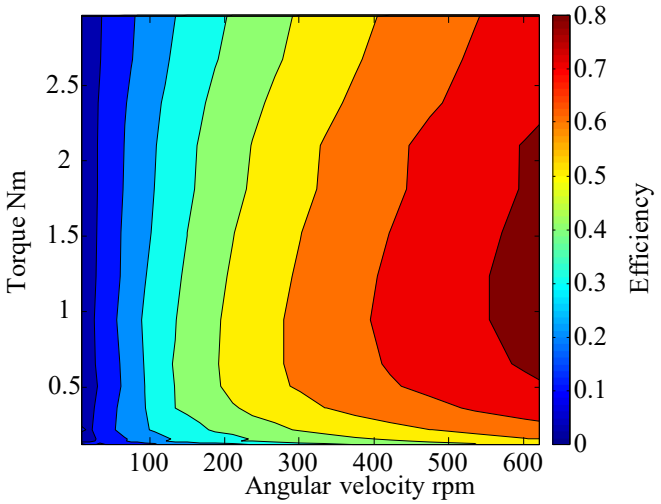

Figure 7 Motor efficiency map of example conditions listed in Figs. 5 and 6 (Type A coupling, K_{vp} = 0.15)

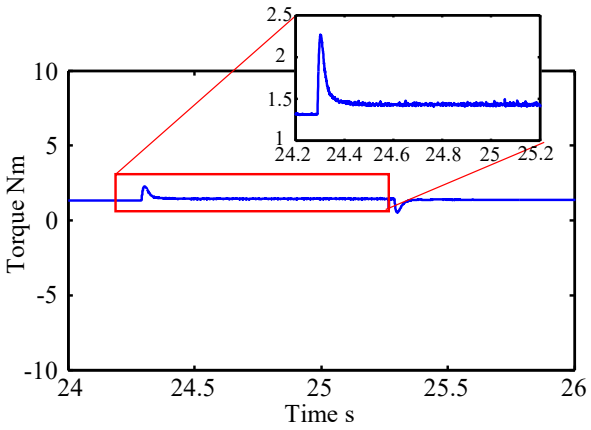

(a) K_{vp} : 0.10

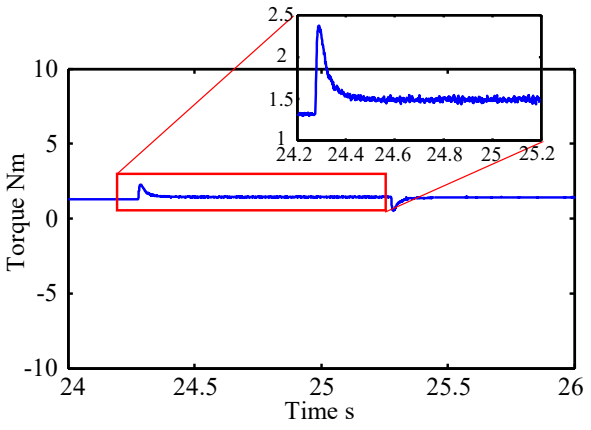

(b) K_{vp} : 0.15

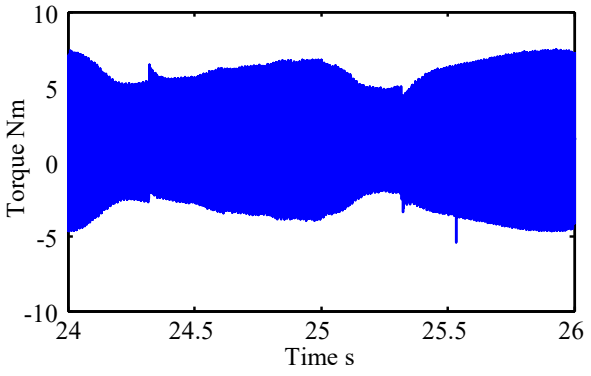

(c) K_{vp} : 0.30

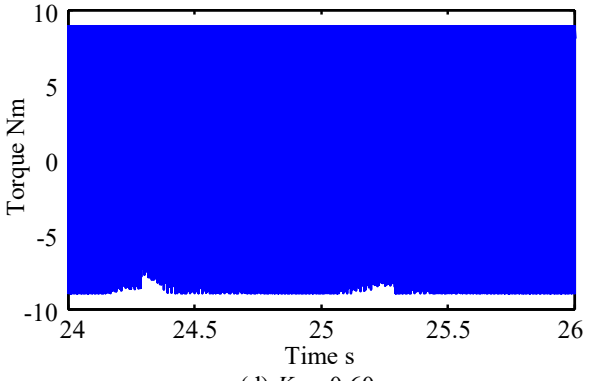

(d) K_{vp} : 0.60

Figure 8 Comparison of torque signals at different K_{vp} values (Type A coupling)

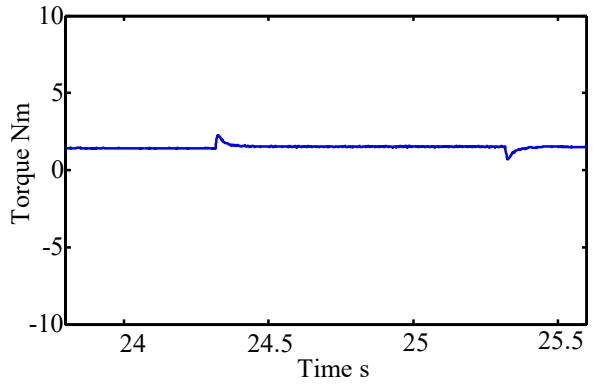

(a) K_{vp} : 0.10

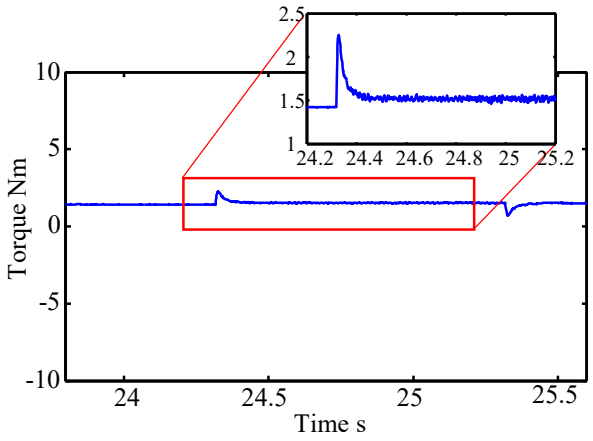

(b) K_{vp} : 0.15

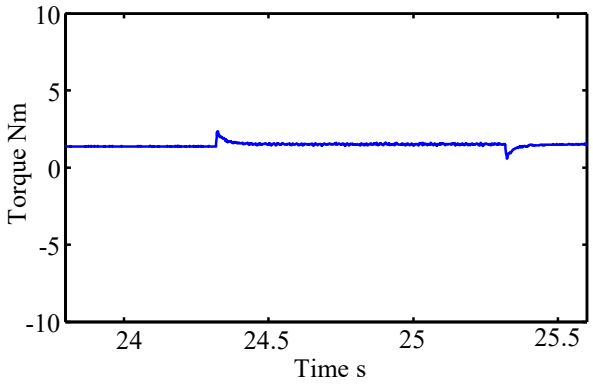

(c) K_{vp} : 0.30

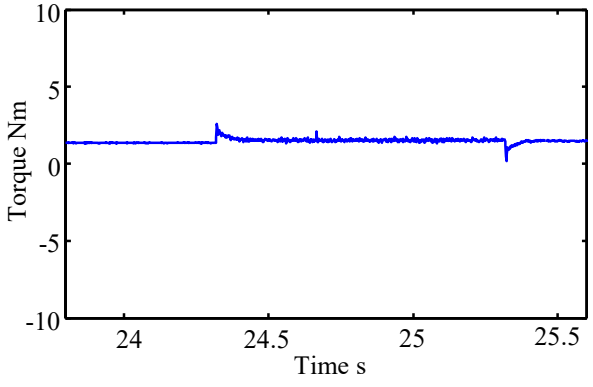

(d) K_{vp} : 0.60

Figure 9 Torque signal comparison at different K_{vp} values (Type B coupling)

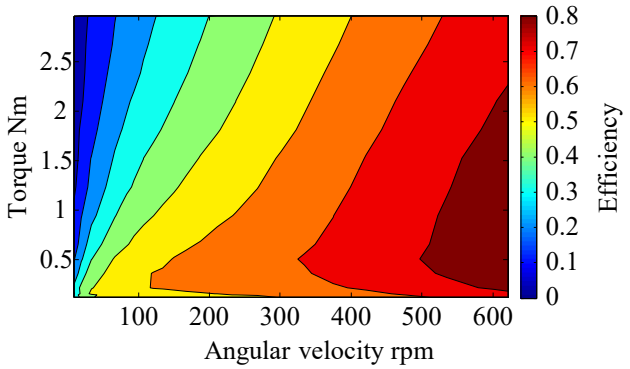

(a) Type A coupling

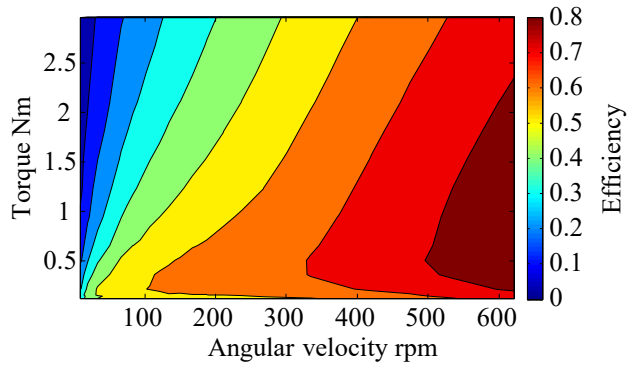

(b) Type B coupling

Figure 10 Comparison of coefficient map of the motor with different couplings (K_{vp} = 0.10)

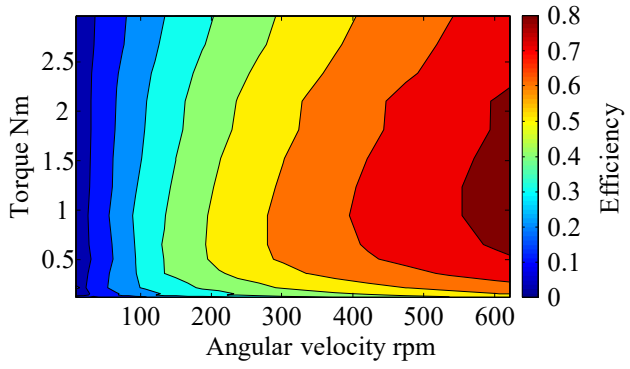

(a) Type A coupling

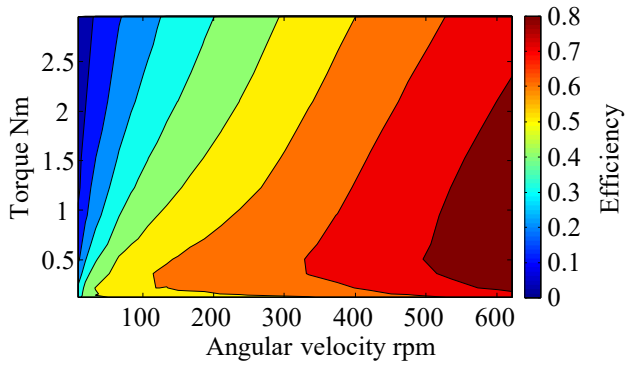

(b) Type B coupling

Figure 11 Comparison of coefficient map of the motor with different couplings (K_{vp} = 0.15)

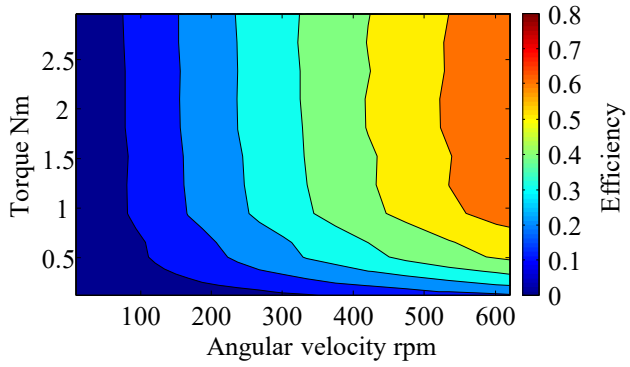

(a) Type A coupling

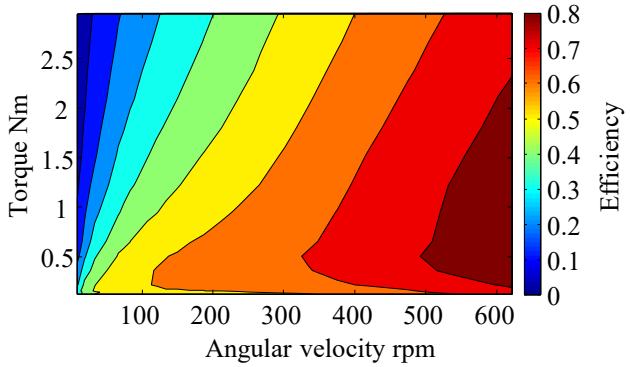

(b) Type B coupling

Figure 12 Comparison of coefficient map of the motor with different couplings (K_{vp} = 0.30)

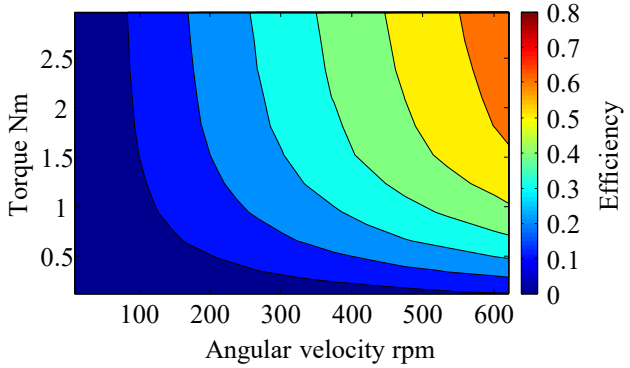

(a) Type A coupling

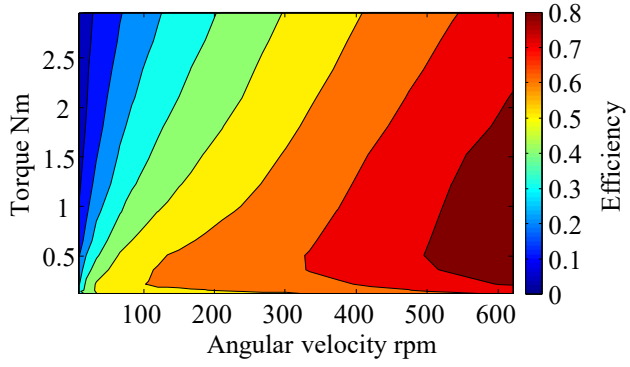

(b) Type B coupling

Figure 13 Comparison of coefficient map of the motor with different couplings (K_{vp} = 0.60)

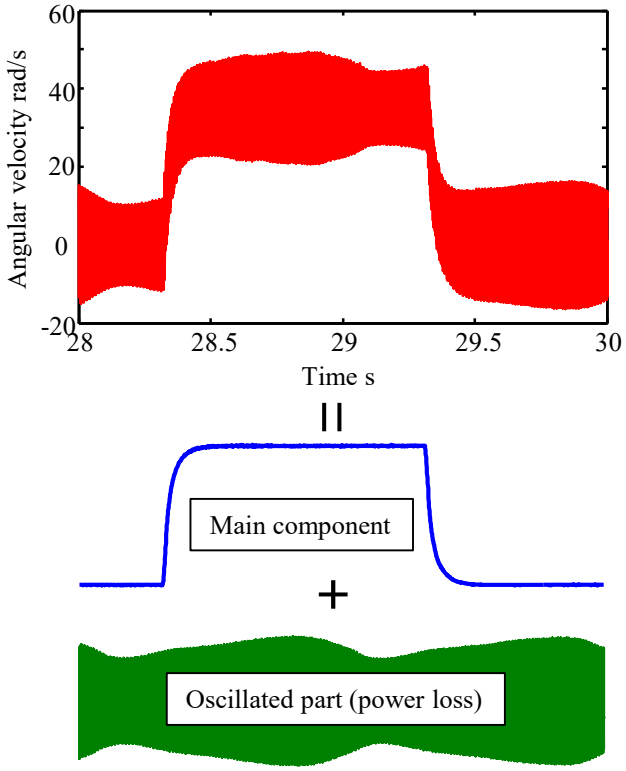

Figure 14 Schematics of the main and oscillating components during motion (K_{vp}= 0.30)

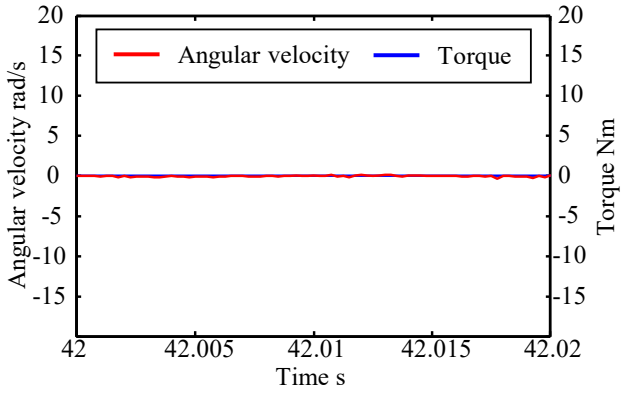

(a) K_{vp} : 0.10

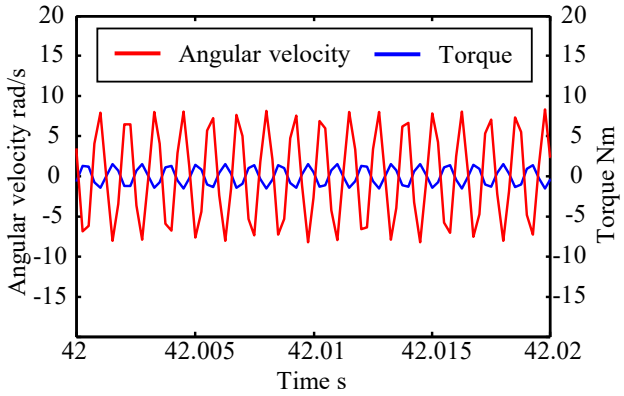

(b) K_{vp} : 0.15

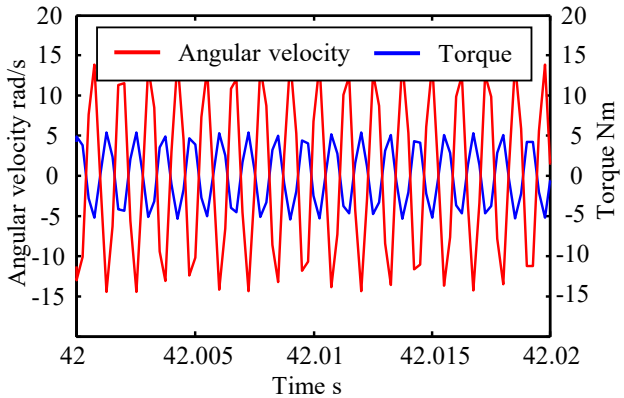

(c) K_{vp} : 0.30

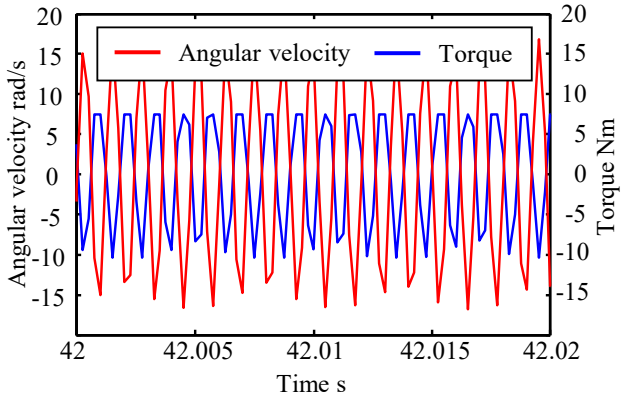

(d) K_{vp} : 0.60

Figure 15 Oscillating component comparison at different K_{vp} values (Type A coupling)

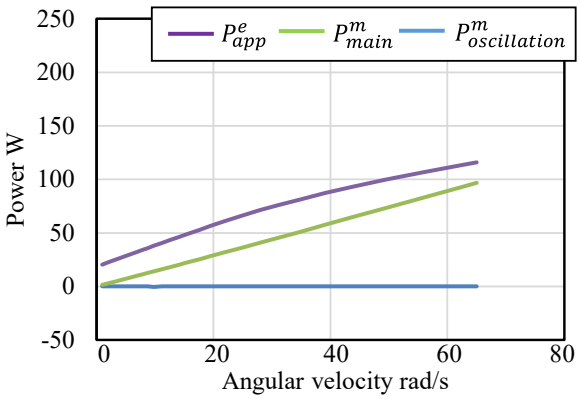

(a) K_{vp} : 0.10

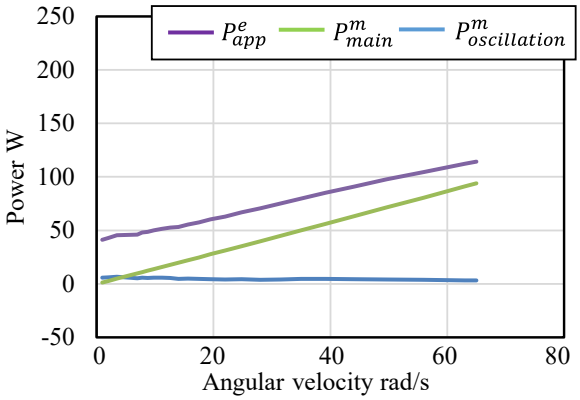

(b) K_{vp} : 0.15

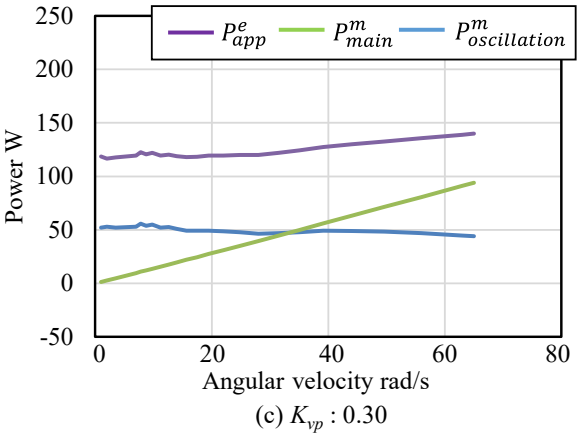

(c) K_{vp} : 0.30

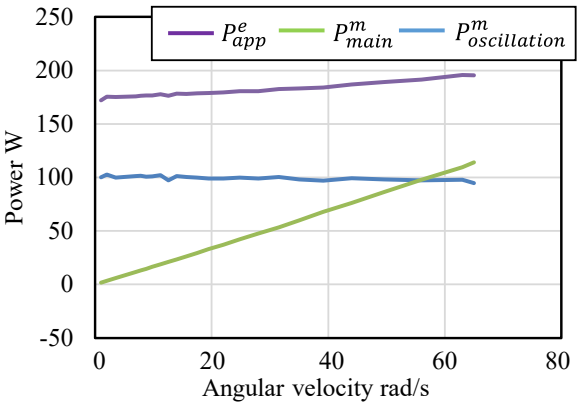

(d) K_{vp} : 0.60

Figure 16 Power flux analysis for each component at different K_{vps} values (Type A coupling)

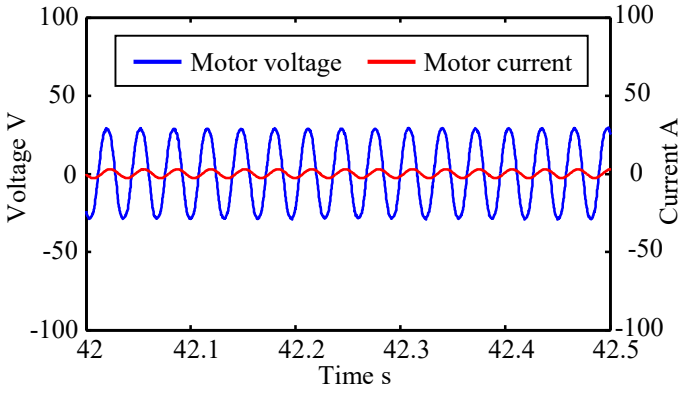

(a) K_{vp} : 0.15

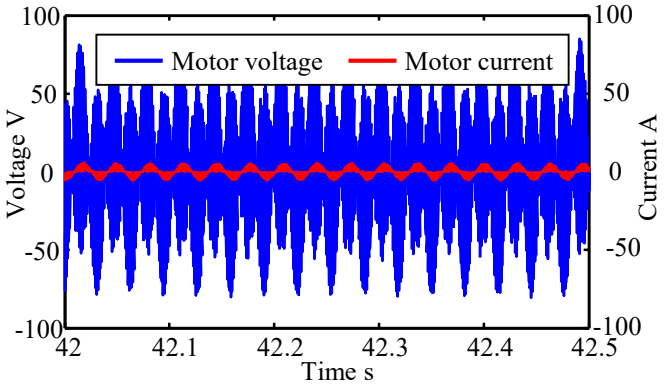

(b) K_{vp} : 0.60

Figure 17 Voltage and current wave form comparison at different K_{vp} values (Type A coupling)

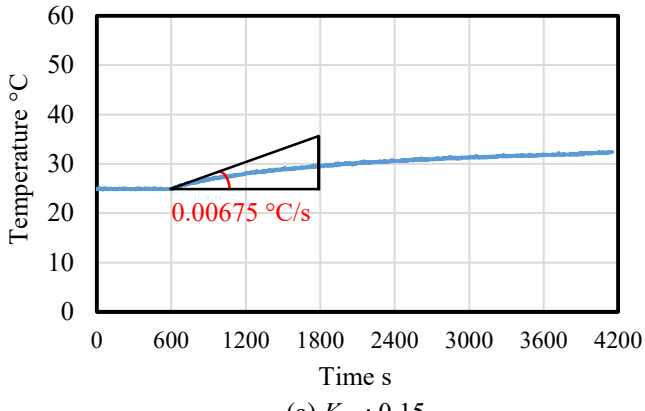

(a) K_{vp} : 0.15

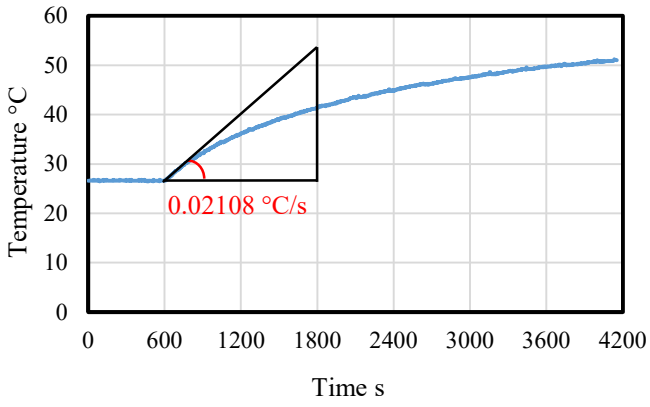

(b) K_{vp} : 0.60

Figure 18 Temperature increase at different motor efficiency levels; angular velocity = 250 rpm, supplied torque = 1 Nm (see Figure 10 (a) and Figure 13 (a) for efficiency)